Molecular Structure – Activity Relationships for the Oxidation of Organic Compounds Using Mesoporous Silica Catalysts Derivatised with Bis(halogeno)dioxomolybdenum(VI) Complexes

Carla D. Nunes, Anabela A. Valente, Martyn Pillinger, João Rocha, and Isabel S. Gonçalves*[a]

Abstract: Mo *K*-edge XAFS spectra have been measured for ordered mesoporous silica MCM-41 grafted with the complexes $[MoO_2X_2(thf)_2]$ (X = Cl, Br). For grafting reactions in the absence of triethylamine, materials with 1 wt.% Mo are obtained; the Mo *K*-edge EXAFS results indicate the co-existence of isolated surface-fixed monomeric species $\{MoO_2[(-O)_3SiO]_2(thf)_n\}$ and $\{MoO_2[(-O)_3SiO]X(thf)_n\}$. When Et_3N is used in the grafting reactions, materials with 4 wt.% Mo are obtained. The EXAFS data for the material prepared using $[MoO_2Cl_2(thf)_2]$ and Et_3N indicate the presence of dinuclear species with two Mo^{VI} centres, each with two Mo=O groups and each linked by one or two oxo bridges (Mo···Mo 3.27 Å). The molybdenum centres in the material prepared using the dibromo complex comprise mainly isolated four-coordinate dioxomolybdenum(VI) and trioxomolybdenum(VI) monomeric species, with a small contribution from dimeric species. All materials were further characterised in the solid state by powder X-ray diffraction, N_2 adsorption analysis, MAS NMR (^{13}C, ^{29}Si) and FTIR spectroscopy. The derivatised MCMs perform differently as catalysts in the liquid-phase oxidation of various olefins and alcohols with *tert*-butyl hydroperoxide. The highest alkene epoxidation activity was recorded for the catalysts with low metal loading, whereas the material containing oxo-bridged dimers had the highest activity for oxidation of alcohols. The recyclability of all the catalysts was tested: the catalytic activity of the derivatised materials tended to stabilize with ageing.

Keywords: EXAFS spectroscopy · heterogeneous catalysis · mesoporous materials · molybdenum · oxidation

Introduction

Silica and alumina substrates have been used for decades to support transition-metal oxides for catalytic applications.[1] These supports are attractive for their high specific surface area, mechanical stability and promotion of well-dispersed active sites.[2] In the last ten years or so, micelle-templated inorganic oxides have emerged as promising alternatives[3] mainly because, in addition to the characteristics mentioned above, they exhibit an ordered array of uniform mesopores that permit catalytic reactions in constrained environments (for example, those involving bulky substrate and/or product molecules).[4] Most of the work has been with silica-based materials, in particular hexagonal mesoporous silicas such as MCM-41,[5] SBA-3[6] and FSM-16,[7] and cubic mesoporous silicas such as MCM-48[5] and SBA-1.[6] Like those of the commonly used silica and alumina supports, the internal surfaces of these materials contain reactive silanol groups that can be used to prepare derivatised materials.[8] Functionalisation of ordered mesoporous silicas with transition-metal oxides has been of particular interest. One approach is to graft organometallic or metal-organic complexes onto the support; this is followed by calcination to produce isolated oxo–metal species. Suitable precursors include metal alkoxides[9] or metallocenes.[10] The preparation of isolated Mo^{VI} active sites on ordered mesoporous silica is especially interesting, given that silica-supported molybdenum oxides are widely used for a variety of selective oxidative dehydrogenations such as the oxidation of methane to methanol and formaldehyde.[11] Some of us recently reported a convenient one-step procedure for the preparation of Mo^{VI} active sites on MCM-41 and MCM-48,[12] involving direct grafting of complexes $[MoO_2X_2(thf)_2]$ (X = Cl, Br) onto the purely siliceous supports using dichloromethane as solvent. A subsequent calcination step was not necessary. Preliminary tests showed that the grafted materials were active as catalysts for the epoxidation of cyclooctene with *tert*-butyl hydroperoxide (TBHP) as the oxidant. It was assumed that the active sites were surface-fixed monomeric species $\{MoO_2[(-O)_3SiO]X(thf)_n\}$, although we had no direct spectroscopic evi-

[a] Dr. I. S. Gonçalves, C. D. Nunes, Dr. A. A. Valente, Dr. M. Pillinger, Prof. Dr. J. Rocha
Department of Chemistry, CICECO, University of Aveiro
Campus de Santiago, 3810-193 Aveiro (Portugal)
Fax: (+351) 234-370084
E-mail: igoncalves@dq.ua.pt

DOI: 10.1002/chem.200304887

dence to support this conclusion (the materials were characterised by elemental analysis, powder X-ray diffraction (XRD), N_2 adsorption, and magic-angle spinning (MAS) NMR spectroscopy). In the present work, Mo *K*-edge X-ray absorption fine structure (XAFS) spectroscopy and IR spectroscopy have been used to probe the local structure of supported Mo species in MCM-41 grafted with the bis(halogeno)dioxomolybdenum(VI) complexes. We have also studied the effect of using triethylamine in the grafting reactions to activate the surface silanols and to sequester the HCl liberated, and we report in detail on the activities of the derivatised materials as catalysts for liquid-phase epoxidation of cyclooctene with TBHP as the oxygen source, and the oxidation of alcohols. The differences in the observed catalytic behaviour are correlated with the variability in the structures of the supported oxomolybdenum catalysts.

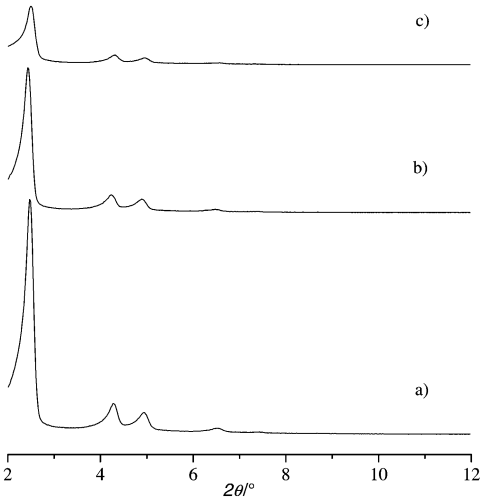

Figure 1. Powder XRD patterns of a) MCM-41, b) MCM-41/**1** and c) MCM-41/**1**/Et_3N. Similar results were obtained for MCM-41/**2** and MCM-41/**2**/Et_3N.

Results and Discussion

Textural characterisation: The MCM-41 sample was of higher quality than the one used previously for grafting reactions with complexes $[MoO_2X_2(thf)_2]$ (X = Cl (**1**), Br (**2**)).[12] Five reflections that were observed in the powder X-ray diffraction pattern (Figure 1) were indexed, assuming a hexagonal cell, as (100), (110), (200), (210) and (300). The *d* value of the (100) reflection is 35.7 Å, giving a lattice constant of $a = 41.2$ Å. Treatment of calcined and dehydrated MCM-41 with a dichloromethane solution of **1** or **2** (in excess) gave derivatised materials with a metal loading of about 1 wt.% (0.1 mmol g^{-1}). This is the maximum that can be achieved in the absence of agents to activate the surface silanol groups. The loading corresponds to a surface coverage of 0.1 atoms nm^{-2} (assuming the metal atom layer thickness to be negligible and an average support surface area of 800 $m^2 g^{-1}$). For comparison, the approximate abundance of silanol groups on calcined MCM-41 has been reported to be in the range 1–3 nm^{-2};[13] of these about 25% are free silanols (involving single and geminal groups), and the rest are hydrogen-bonded.[13a] Zhao et al. showed that only the free silanol groups on MCM-41 are readily accessible to the silylating agent, chlorotrimethylsilane.[13a] It can be assumed therefore that the molybdenum complexes react only with free silanol groups. The powder XRD patterns for the grafted materials MCM-41/**1** and MCM-41/**2** were quite similar to that of pristine calcined MCM-41 (Figure 1), which indicates retention of the long-range hexagonal symmetry. There was a slight attenuation of XRD peak intensities. This is not interpreted as a loss of crystallinity. Instead, it is likely that there is a reduction in the X-ray scattering contrast between the silica wall and pore-filling material.[14] When triethylamine (Et_3N) was used in the grafting reactions, materials with a much higher metal loading were obtained (approximately 4 wt.% Mo, 0.4 mmol g^{-1}), corresponding to a surface coverage of 0.3 atoms nm^{-2} (assuming an average support surface area of 800 $m^2 g^{-1}$). At least four reflections were observed in the powder XRD patterns of MCM-41/**1**/Et_3N and MCM-41/**2**/Et_3N. The peak intensities were reduced considerably compared with those of MCM-41/**1** or MCM-41/**2**, presumably because of the higher metal loading.

The N_2 adsorption–desorption isotherms for the pristine and modified MCM-41 samples were type IV as defined by IUPAC, characteristic of mesoporous solids. All the isotherms were reversible, with clear capillary condensation steps indicating that the textural characteristics of the silica support are preserved during the grafting experiments and that the channels remain accessible. Figures 2 and 3 show isotherms for MCM-41 before and after derivatisation of the silica surface, with and without triethylamine treatment. The modifications led to a decrease in the limiting N_2 uptake at high p/p_0, and both the surface area and pore volume decreased (Table 1). The plot of differential volume as a function of pore width shows a relatively narrow pore size distribution (PSD), with median pore diameters ranging from 2.9 to 3.2 nm for pristine MCM-41 and 2.6 to 3.2 nm for the modified samples. The grafting procedure without Et_3N caused an increase in the width at half-height, indicating an increase in pore heterogeneity (Figure 2). For the catalysts prepared using Et_3N, a shift of the maximum of the PSD curve from 2.9 to 2.6 nm was observed upon surface modification (Figure 3).

Spectroscopic characterisation: Figure 4 shows the ^{29}Si MAS and CP-MAS NMR spectra of pristine MCM-41, MCM-41/**1** and MCM-41/**1**/Et_3N. The ^{29}Si MAS spectrum of the starting material exhibits two broad overlapping peaks at $\delta = -102.0$ and -109.0 ppm assigned to, respectively, Q^3 and Q^4 units of the silica framework ($Q^n = Si(OSi)_n(OH)_{4-n}$). A small proportion of Q^2 environments is also present (there is a faint peak at $\delta = -92.5$ ppm). The ^{29}Si CP-MAS NMR spectrum shows a marked increase in the relative intensity of the Q^2 and Q^3 lines in comparison with the ^{29}Si MAS spectrum, confirming that these silicons are attached to hydroxyl groups. In agreement with those previously reported,[12] both the ^{29}Si CP-MAS and MAS NMR spectra show that upon functionalisation with **1** in the absence of Et_3N, the relative intensity of the

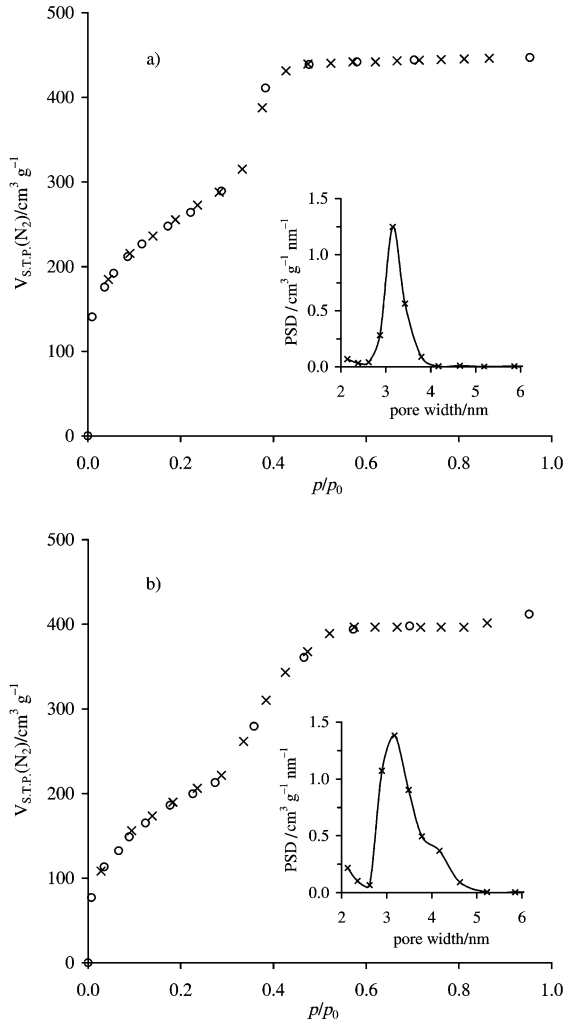

Figure 2. Nitrogen adsorption (○) – desorption (×) isotherms at 77 K of a) the parent MCM-41 and b) MCM-41/**1**, and the corresponding pore size distribution (PSD) profiles.

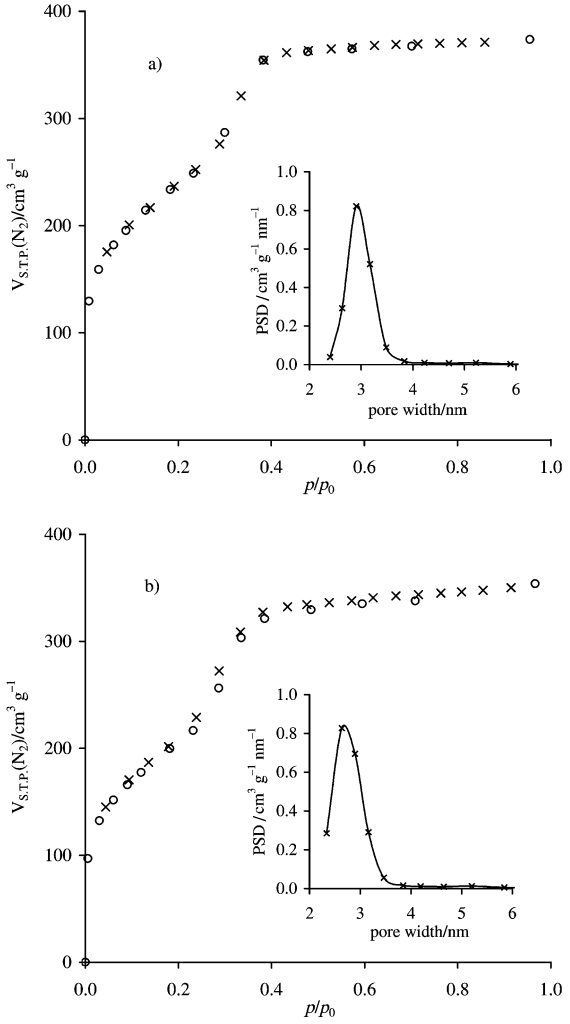

Figure 3. Nitrogen adsorption (○) – desorption (×) isotherms at 77 K of a) the parent MCM-41 and b) MCM-41/**1**/Et_3N, and the corresponding pore size distribution (PSD) profiles.

Q^3 (and Q^2) peak(s) changes only slightly, consistent with the low metal loading (approximately 1 wt.% Mo). For the material prepared in the presence of triethylamine, the ^{29}Si CP-MAS NMR spectrum clearly shows a reduction in the Q^3 and Q^2 resonances, and a concomitant increase in the Q^4 resonance. This indicates an extensive interaction of surface silanols with triethylamine and/or the grafted molybdenum species (consistent with the higher metal loading). The materials MCM-41/**2** and MCM-41/**2**/Et_3N exhibited similar ^{29}Si NMR spectra to those of MCM-41/**1** and MCM-41/**1**/Et_3N, respectively (not shown). In the ^{13}C CP-MAS NMR spectra of MCM-41/**1** and MCM-41/**2** (not shown), lines observed at $\delta =$ 24.7 and 68.0 ppm are assigned to coordinated THF molecules. By contrast, ^{13}C CP-MAS NMR showed that the grafted materials MCM-41/**1**/Et_3N and MCM-41/**2**/Et_3N do not contain THF, but do contain triethylammonium ions (lines at 7.6 and 46.6 ppm).

The precursor MCM-41 samples and derivatised materials were also characterised by FTIR spectroscopy. Pristine calcined MCM-41 presented a spectrum comparable with that of MCM-48.[9f] Two framework bands for the asymmetric stretch (ν_{as}) of the Si – O – Si bonds are observed at 1235 and 1087 cm^{-1}, with a weak peak at 1180 cm^{-1}. A strong peak at 800 cm^{-1} is attributed to ν_{sym} of the Si – O – Si bonds while a broad band at 570 cm^{-1} is ascribed to the "crystallinity peak" in zeolite synthesis, indicative of the formation of an ordered network solid.[9f] An absorption at 963 cm^{-1} is assigned to the $Si-O^{\delta-}$ of a Si – OH stretch. When MCM-41 was grafted with **1** or **2** in the absence of Et_3N, these bands due to the support did not change significantly in appearance or frequency. Several new bands were observed; they are assigned to the grafted species and/or their interaction with the host. The

Table 1. Textural parameters of MCM-41 samples determined from N_2 isotherms at 77 K.

Sample	S_{BET} [m^2g^{-1}]	ΔS_{BET}[a] [%]	V_P [cm^3g^{-1}]	ΔV_P[b] [%]	d_P [nm]
MCM-41-1	928	–	0.69	–	3.2
MCM-41/**1**	734	– 21	0.64	– 7	3.2
MCM-41/**2**	855	– 8	0.67	– 3	3.2
MCM-41-2	863	–	0.58	–	2.9
MCM-41/**1**/Et_3N	760	– 12	0.55	– 5	2.6
MCM-41/**2**/Et_3N	652	– 24	0.46	– 21	2.6

[a] Variation of surface area in relation to parent MCM-41. [b] Variation of total pore volume in relation to parent MCM-41.

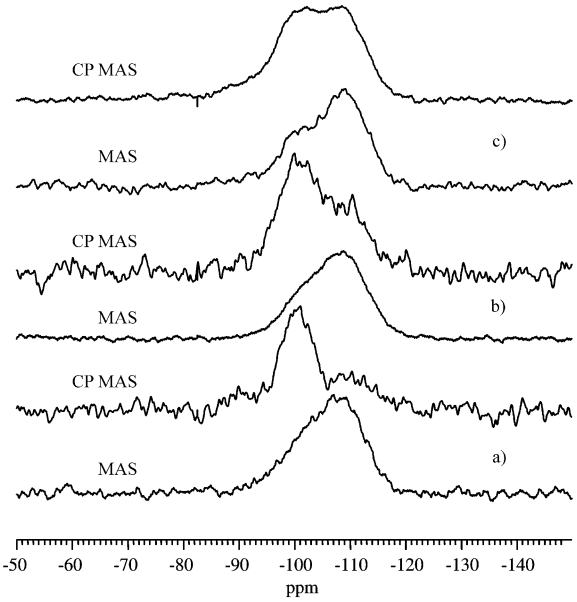

Figure 4. ^{29}Si MAS and CP-MAS NMR spectra of a) MCM-41, b) MCM-41/**1** and c) MCM-41/**1**/Et_3N.

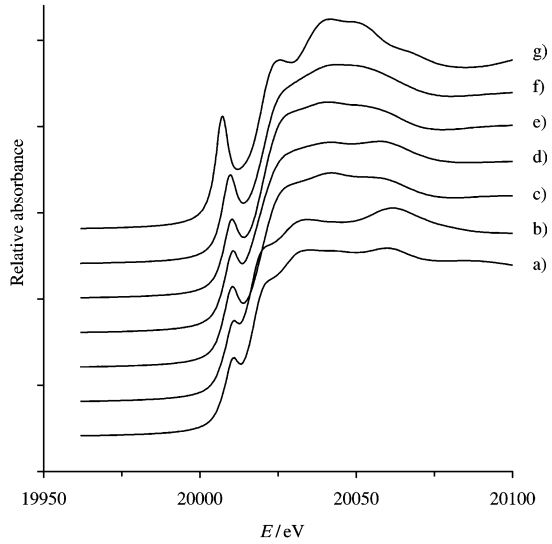

Figure 5. Mo *K*-edge XANES spectra of a) $[MoO_2Cl_2(thf)_2]$ (**1**), b) $[MoO_2Br_2(thf)_2]$ (**2**), c) MCM-41/**1**, d) MCM-41/**2**, e) MCM-41/**1**/Et_3N, f) MCM-41/**2**/Et_3N and g) $Na_2MoO_4 \cdot 2H_2O$.

presence of THF is indicated by bands at 2890 and 2980 cm^{-1}. A weak shoulder at 918 cm^{-1} may be due to the asymmetric stretch of the C–O–C bonds of THF or to a Mo=O stretching vibration (the latter usually occurs at $\geq$900 cm^{-1} for *cis*-dioxomolybdenum(VI) complexes). A second shoulder at about 890 cm^{-1} is assigned to a Mo=O stretching vibration. For comparison, the Mo=O stretching vibrations for the precursor complex **2** appear at 904 cm^{-1} (asymmetric) and 942 cm^{-1} (symmetric). The FTIR spectra of MCM-41/**1**/Et_3N and MCM-41/**2**/Et_3N show bands due to triethylammonium ions (1398, 1475, 2492, 2690, 2726, 2790 and 2990 cm^{-1}). The absorption at 965 cm^{-1} due to the $Si-O^{\delta-}$ of a Si–OH stretch is reduced to a weak intensity and a new band appears at 945 cm^{-1}. In agreement with the ^{29}Si NMR results, this indicates a strong interaction of a large fraction of the surface silanols with triethylamine and/or oxomolybdenum species. Both samples also exhibit a shoulder at 918 cm^{-1} that is assigned to a Mo=O stretching vibration (the ^{13}C CP-MAS NMR spectra showed that the samples do not contain THF). The grafted material MCM-41/**1**/Et_3N (but not MCM-41/**2**/Et_3N) exhibits a prominent shoulder at 885 cm^{-1}. Considering the Mo *K*-edge EXAFS data (described below), this band is tentatively assigned to a Mo–O–Mo stretching vibration (usually expected in the range 700–900 cm^{-1}).

EXAFS spectroscopy is perhaps the best technique to probe the molecular structure of the molybdenum centres in the grafted materials. However, where structural diversity of metal species arises, the traditional approach to modelling the resultant EXAFS spectrum can give only an indication of the average structural environment. Mo *K*-edge X-ray absorption spectra were collected at room temperature in the solid state for the precursor complexes **1** and **2**, and the four derivatised materials. The XANES data are shown in Figure 5. The spectra for the precursor complexes are quite similar, both exhibiting a rather weak pre-edge feature that is attributed to a bound state transition ($1s \rightarrow 4d$). The intensity of this peak is usually strongest for molybdenum coordination systems with non-inversion symmetry, such as tetrahedral geometry.[15] Sodium molybdate, for example, exhibits an intense well-resolved pre-edge peak (Figure 5). Any distortion of the regular tetrahedral symmetry leads to a decrease in the peak intensity. The XANES spectra of complexes **1** and **2** are therefore consistent with the expected molybdenum coordination, that is, distorted octahedral geometry. The clear differences in both amplitude and frequency between the XANES oscillations of the precursor complexes and derivatised materials demonstrate that the grafting process has imposed changes in the local structural order around the molybdenum centres. The increase in the intensity of the pre-edge peak for the grafted materials indicates a change in the molybdenum coordination geometry. Enhancement of this transition has also been associated with an increasing number of Mo=O bonds.[16]

Good quality EXAFS spectra were obtained up to 16–20 $Å^{-1}$ for all the compounds examined. Analysis of the EXAFS for **1** and **2** gave the expected first coordination spheres of two oxygen atoms at 1.69–1.70 Å ($Mo-O_t$), approximately two oxygen atoms at 2.24–2.26 Å ($Mo-O_{THF}$) and two halogen atoms at either 2.36 Å (Cl) or 2.52 Å (Br) (Figures 6 and 7; Table 2). The $Mo-O_t$ and Mo–X distances are in agreement with those obtained by single-crystal X-ray diffraction for Lewis base adducts $[MoO_2X_2L_2]$ (L_2 = 2,2′-bipyridine, 2,2′-bipyrimidine).[18] If **1** was grafted into MCM-41 (MCM-41/**1**), a substantially different model was required for a reasonable fit to the Mo *K*-edge EXAFS, comprising oxygen shells at 1.70, 1.93 and 2.24 Å (Figure 6b). The first shell is extremely well defined and confirms the presence of dioxo species. The appearance of the new shell at 1.93 Å, coupled with the fact that no acceptable fit could be obtained for a chlorine shell at approximately 2.35 Å, is consistent with the formation of Mo–O–Si linkages (by reaction of the complex with nucleophilic surface silanol groups) (Figure 8). The refined coordination number for the

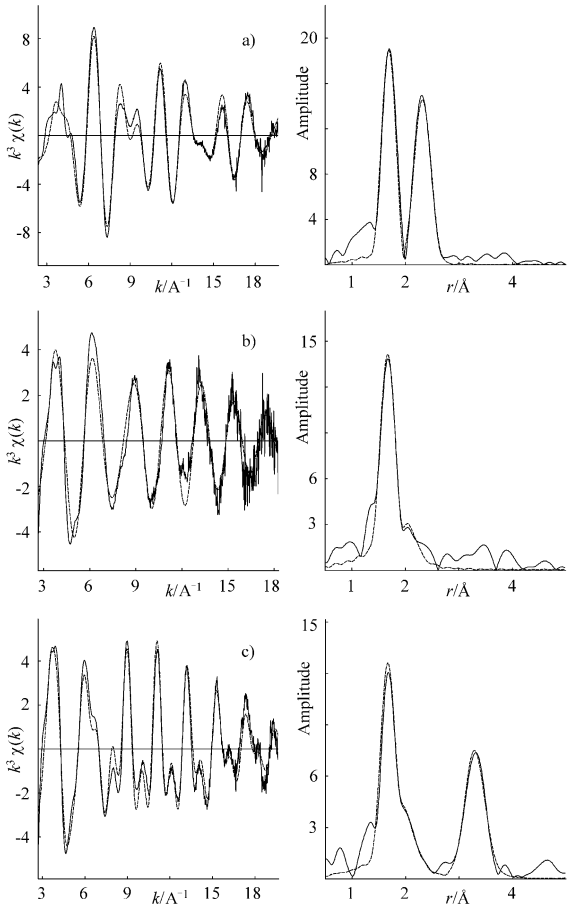

Figure 6. Room-temperature Mo *K*-edge EXAFS and Fourier transforms of a) **1**, b) MCM-41/**1** and c) MCM-41/**1**/Et_3N. The solid lines represent the experimental data and the broken lines show the best fits using the parameters given in Table 2.

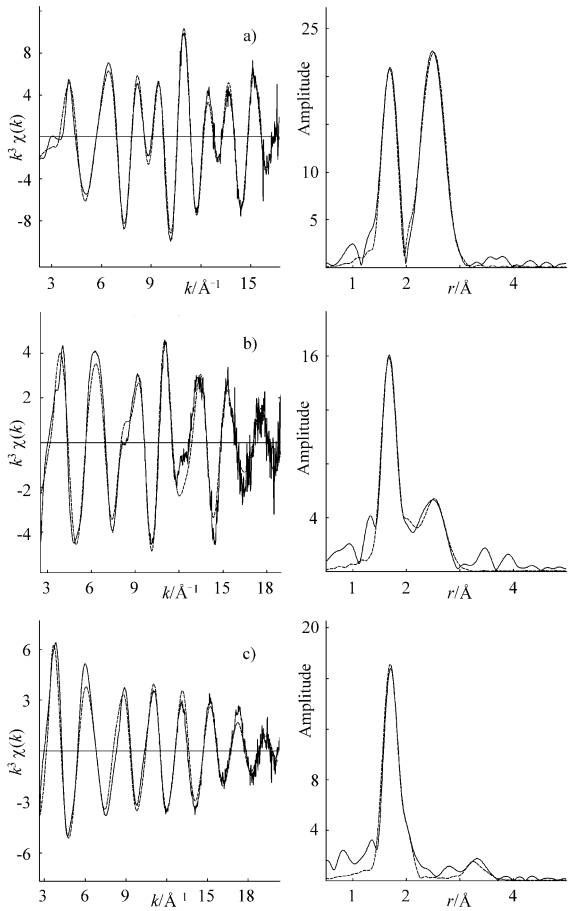

Figure 7. Room-temperature Mo *K*-edge EXAFS and Fourier transforms of a) **2**, b) MCM-41/**2** and c) MCM-41/**2**/Et_3N. The solid lines represent the experimental data and the broken lines show the best fits using the parameters given in Table 2.

second oxygen shell is close to 1, lower than the expected value of 2 for a bipodally anchored species. Static disorder in the Mo – O_b bonds may account for this discrepancy. Refinement of coordination numbers and Debye – Waller factors simultaneously does not always give reliable results, owing to the high correlation of the two parameters. Attempts to model a Mo···Si distance (in the range 3 – 4 Å) corresponding to a Mo – O – Si linkage were unsuccessful. This may again be due to disorder in the Mo – O – Si interactions. There are still THF molecules coordinated to the Mo^{VI} centre, as evidenced by the shell at 2.24 Å (in agreement with the ^{13}C CP-MAS NMR results). In the case of MCM-41 grafted with the dibromo complex **2** (MCM-41/**2**), three oxygen shells were again in evidence, corresponding to Mo – O_t, Mo – O_b and Mo – O_{THF} bonds. A fourth shell for bromine atoms was also included in the final fit (coordination number = 0.6). The EXAFS results for the grafted materials therefore indicate the coexistence of isolated surface-fixed monomeric species $\{MoO_2[(-O)_3SiO]_2(thf)_n\}$ (site A) and $\{MoO_2[(-O)_3SiO]X(thf)_n\}$ (site B) (Figure 8). The relative population of monopodally anchored species (B) seems to be higher for the grafted material MCM-41/**2**, consistent with the greater lability of the Cl ligands than the Br ligands in the precursor complexes **1** and **2**.

Table 2. Mo *K*-edge EXAFS-derived structural parameters for **1**, **2** and derivatised MCM-41 materials.

Compound	Atom	CN[a]	r [Å]	$2\sigma^2$[b] [Å^2]	E_f[c] [eV]	R[d] [%]
1	O	2.0(1)	1.692(2)	0.0023(2)	– 1.2(7)	26.2
	O	2.5(7)	2.242(13)	0.0257(51)		
	Cl	1.8(2)	2.355(2)	0.0053(3)		
2	O	2.1(1)	1.696(2)	0.0022(2)	– 3.4(6)	18.0
	O	2.2(3)	2.262(7)	0.0114(16)		
	Br	1.8(1)	2.515(2)	0.0055(2)		
MCM-41/**1**	O	2.0(1)	1.695(2)	0.0044(3)	4.3(7)	31.2
	O	1.0(2)	1.927(7)	0.0076(14)		
	O	1.4(4)	2.240(15)	0.0210(49)		
MCM-41/**2**	O	2.0(1)	1.689(2)	0.0036(2)	1.5(7)	28.6
	O	1.0(3)	1.929(6)	0.0061(10)		
	O	2.0(5)	2.275(13)	0.0262(47)		
	Br	0.6(1)	2.526(5)	0.0084(7)		
MCM-41/**1**/Et_3N	O	2.0(1)	1.695(2)	0.0048(2)	5.4(4)	25.9
	O	1.5(2)	1.924(4)	0.0101(10)		
	Mo	1.4(2)	3.274(3)	0.0083(3)		
	O	0.8(2)	2.310(14)	0.0127(36)		
MCM-41/**2**/Et_3N	O	2.5(1)	1.714(2)	0.0043(2)	4.1(4)	25.8
	O	1.0(1)	1.940(4)	0.0043(7)		
	Mo	0.3(2)	3.255(14)	0.0093(23)		

[a] CN = Coordination number. Values in parentheses are statistical errors generated in EXCURVE. The true errors in coordination numbers are likely to be of the order of 20%, and those for the interatomic distances ≈1.5%.[17] [b] Debye – Waller factor; σ = root-mean-square internuclear separation. [c] E_f = edge position (Fermi energy), relative to calculated vacuum zero. [d] $R = (\int[\Sigma^{theory} - \Sigma^{exptl}]k^3 dk/[\Sigma^{exptl}]k^3 dk) \times 100\%$.

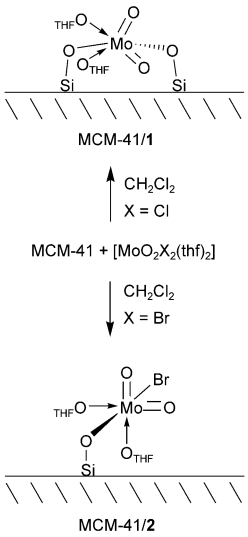

Figure 8. Representation of the predominant species present in MCM-41 derivatised with the complexes **1** and **2** in the absence of Et_3N, as evidenced by Mo *K*-edge XAFS spectroscopy.

The inclusion of triethylamine in the grafting reaction of $[MoO_2Cl_2(thf)_2]$ with MCM-41 results in an EXAFS spectrum that is very different from that of MCM-41/**1** (Figure 6c). An intense new peak is present in the Fourier transform (FT) above 3 Å. This was best modelled as 1.4 molybdenum atoms at 3.27 Å. In the final fit, 1.69, 1.92 and 2.31 Å Mo–O distances were also included (Table 2). The goodness-of-fit *R* factor decreased from 27.6 to 25.9% upon addition of the oxygen shell at 2.31 Å. A similar improvement in the fit was obtained by fitting one nitrogen at 2.34 Å instead of the oxygen shell at 2.31 Å. Therefore the presence of coordinated triethylamine molecules cannot be ruled out. No evidence was found for a shell at approximately 2.25 Å for coordinated THF molecules. The results indicate that the Mo centres formed in MCM-41/**1**/Et_3N are largely dinuclear species with two Mo^{VI} centres, each with two Mo=O groups and each linked by one or two oxo bridges (Figure 9). Mono-oxo-bridged $[Mo_2O_5]^{2+}$ entities, for example, oxalate complexes $M_2[Mo_2O_5(C_2O_4)_2(H_2O)_2]$ (M = Na, K, Rb, Cs), are quite common in oxomolybdenum(VI) chemistry.[19] Dioxo-bridged fragments $[Mo_2O_6]$ with Mo···Mo 3.27 Å have been structurally characterised in catalysts prepared by immobilisation of species derived from $[MoO_2(acac)_2]$ on a polystyrene *N*-hydroxypropyl aminomethylpyridine resin.[20] The EXAFS-derived coordination number for the Mo···Mo shell is clearly higher than the ideal value of 1 for a dimeric species. It was thought that this might be due to multiple scattering involving the Mo–O_b–Mo unit, despite the rather acute Mo–O–Mo angle (approximately 117° assuming equal Mo–O_b bond lengths of 1.92 Å). However, inclusion of multiple scattering in the calculations for the Mo–O_b–Mo unit (with the coordination numbers fixed at 1.0) resulted in a worse fit to the EXAFS. The initial single scattering approach was therefore retained. The FT of the room-temperature Mo *K*-EXAFS of MCM-41/**1**/Et_3N contains a weak peak above 4.5 Å. This was best fitted as about one molybdenum atom at 4.70 Å. The existence of this shell would suggest a contribution from polymeric species in addition to the dimeric species described above (possibly explaining the calculated coordination number of 1.4 for the Mo···Mo shell). However, the shell is not included in the final four-shell model because the improvement in the fit was modest ($R = 25.2\%$) and there were unacceptably large statistical errors in the refined structural parameters (90% in the coordination number, for example).

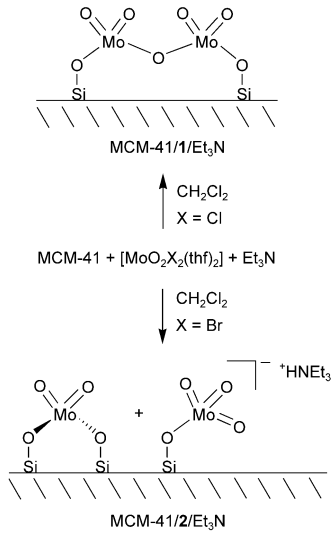

Figure 9. Representation of the predominant species present in MCM-41 derivatised with the complexes **1** and **2** in the presence of Et_3N, as evidenced by Mo *K*-edge XAFS spectroscopy.

The Mo *K*-edge EXAFS results for the grafted material MCM-41/**2**/Et_3N show that the surface chemistry of the dibromo complex is very different from that of the dichloro complex when triethylamine is present to activate the surface silanols. These differences are very evident in both the EXAFS spectra and Fourier transforms (Figure 7). For example, the FT of the Mo *K*-edge EXAFS of MCM-41/**2**/Et_3N contains only a weak peak at about 3.3 Å, compared with the very intense peak observed for the grafted material MCM-41/**1**/Et_3N. The EXAFS data for MCM-41/**2**/Et_3N were initially modelled by oxygen shells at 1.71 Å and 1.94 Å (*R* factor = 27.1%). No acceptable fit could be obtained for a bromine shell at approximately 2.5 Å. A modest improvement in the fit was obtained by addition of a shell for molybdenum atoms (CN = 0.3) at 3.26 Å (*R* factor = 25.8%; Table 2). The contribution of this shell to the overall fit is clearly much less than that observed for the corresponding shell in the fit to the EXAFS of MCM-41/**1**/Et_3N. In fact, a reasonable fit could also be obtained by modelling about one silicon atom at 3.33 Å instead of the molybdenum shell. These results indicate that the surface species in MCM-41/**2**/Et_3N comprise mainly isolated monomers, with perhaps a small contribution from dimers. The EXAFS-derived bond distance and coordination number for the terminal oxo ligands (1.71 Å, 2.5) are significant, since the other grafted materials and precursor complexes **1** and **2** yielded consistent values of 1.695 ± 0.005 Å and 2.0 ± 0.1. The average coordination number of 2.5 suggests the presence of some trioxomolybdenum(VI) species. Anions of the type $[XMoO_3]^-$ are known to exist (in aqueous solution, for example), but very few complexes have been isolated and characterised.[21–23] Arzoumanian et al. obtained crystals of the complex $[PPh_4][Mo(\eta^1\text{-}1,3,5\text{-}C_6H_2Me_3)(O_3)]$ suitable for structure determination by X-ray diffraction.[24] The Mo–O bond lengths were found to be 1.720 ± 0.003 Å. Figure 10 illustrates a possible mechanism for the formation of trioxomolybdenum(VI) species on the surface of MCM-41, starting from an immobilised species $\{MoO_2[(-O)_3SiO]_2\}$.

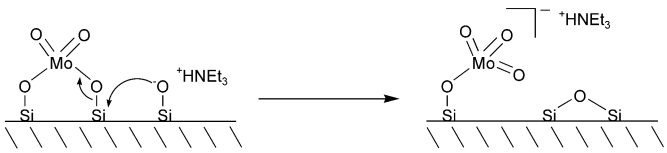

Figure 10. Possible mechanism for the formation of surface-fixed trioxomolybdenum(VI) species in the grafted material MCM-41/**2**/Et_3N.

Catalytic epoxidation of olefins: The behaviour of the derivatised MCM-41 materials as catalysts or catalyst precursors for the liquid-phase epoxidation of olefins was investigated using cyclooctene as a model substrate and *tert*-butyl hydroperoxide (TBHP) as the mono-oxygen source, at 55 °C under air, without additional solvent. All materials catalysed the oxidation of cyclooctene to the corresponding epoxide, and no reaction took place without catalyst. In the first catalytic runs, the systems containing materials MCM-41/**1** and MCM-41/**2** exhibited excellent catalytic activity and selectivity, with conversion of substrate reaching more than 90 % within a few hours (Figure 11; Table 3). This performance was much better than that usually observed in homogeneous-phase reaction for solvent adducts $[MoO_2X_2S_2]$ (X = Cl, Br).[25] For example, under reaction conditions similar to those used in the present work, conversion of cyclooctene in the presence of the dibromo complex $[MoO_2Br_2(CH_3CN)_2]$ quickly reached about 65 % but did not proceed significantly further.[25] This was attributed to the pronounced water sensitivity of the complex.

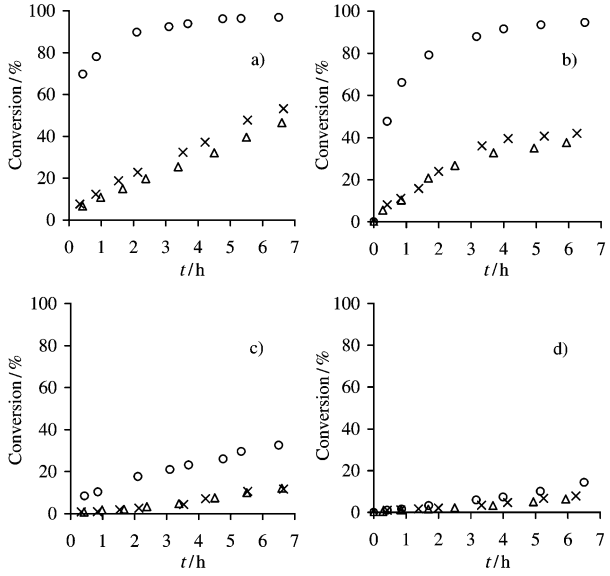

Figure 11. Conversion versus time curves for the oxidation of cyclooctene with TBHP in the presence of a) MCM-41/**1**, b) MCM-41/**2**, c) MCM-41/**1**/Et_3N and d) MCM-41/**2**/Et_3N (○, 1st run; ×, 2nd run; △, 3rd run).

The MCM-41/**1** and MCM-41/**2** samples were prepared according to the procedure described in ref. [12] and had similar molybdenum loadings (approximately 1 wt. %). However, in the present study the catalysts were considerably more active in cyclooctene epoxidation than those prepared in the previous work. This can only be attributed to the much improved long-range structural order (as evidenced by the presence of five reflections in the powder XRD pattern) resulting from the different method by which the host material used here was prepared. The higher catalytic activity may have resulted from improved adsorption characteristics. Oyama et al., for example, reported that the silica surface of silica-supported molybdenum materials participated in the oxidation of methanol by holding reaction intermediates, indicating that the storage capacity of the support can affect the overall activity.[11a]

Table 3. Cyclooctene epoxidation using TBHP in the presence of MCM-41 materials.

Sample	TOF[a] [mmol g^{-1}_{cat} h^{-1}]	Conv.[b] [%]	Selectivity to cyclooctene oxide [%]
MCM-41/**1** (1st run)	38	100	100
MCM-41/**1** (2nd run)	6	86	100
MCM-41/**1** (3rd run)	5	76	100
MCM-41/**2** (1st run)	32	100	100
MCM-41/**2** (2nd run)	6	84	100
MCM-41/**2** (3rd run)	5	72	100
MCM-41/**1**/Et_3N (1st run)	5	56	80[c]
MCM-41/**1**/Et_3N (2nd run)	1	34	94[c]
MCM-41/**1**/Et_3N (3rd run)	1	29	93[c]
MCM-41/**2**/Et_3N (1st run)	1	49	100
MCM-41/**2**/Et_3N (2nd run)	1	27	100
MCM-41/**2**/Et_3N (3rd run)	1	23	100

[a] Turnover frequency calculated after 1 h of reaction. [b] Cyclooctene conversion after 24 h. [c] 1,2-Cyclooctanediol was formed.

The recyclability of MCM-41/**1** and MCM-41/**2** for cyclooctene epoxidation was studied by using the catalysts in second and third reaction runs (Figure 11; Table 3). In both cases a loss of activity was observed from the first to the second runs, while catalytic activity was almost completely retained from the second to the third runs. Selectivity to the epoxide remained very high (Table 3). It is possible that, in the first run, the epoxidation reaction took place within the mesopores of the silica support, involving a relatively small number of highly active oxomolybdenum centres. The active species may have been deactivated (and/or leached into solution) during the course of the reaction, leading to a decrease in activity for the recycled catalyst. As noted above, the catalytic activity and kinetic profiles for the first runs were very different from those usually associated with complexes of the type $[MoO_2X_2(thf)_2]$; this suggests that the ordered mesoporous support still plays a part in the reaction. For the second and third runs the reactions appeared to be truly heterogeneous, involving oxomolybdenum species covalently anchored to the support. For a given catalytic run, the activities of the catalysts derived from either complex **1** or **2** were similar. In accordance with the EXAFS results, this suggests that the halogeno ligands had been at least partially removed during the grafting reactions, since dichloro complexes $[MoO_2Cl_2S_2]$ usually exhibit higher activity (because of the increased electrophilicity of the metal centre) than the corresponding dibromo complexes.[26]

The catalytic performance of MCM-41/**1** was also tested in the epoxidation of other olefins, since cyclooctene has high reactivity and a low tendency towards epoxide opening. The

values of turnover frequency (TOF) and olefin conversion are shown in Figure 12. This catalyst oxidises 1-octene, *trans*-2-octene and cyclododecene with excellent product selectivity, the corresponding epoxide being the only observed product. In the oxidation of α-pinene, pinene oxide and campholenic aldehyde are produced each with 50% selectivity, at 20% conversion. MCM-41/**1** is less reactive towards the terminal carbon–carbon double bond of 1-octene than to a more substituted olefin (with a more nucleophilic double bond) such as *trans*-2-octene. For bulkier substrates such as cyclododecene, the reaction is slower than for cyclooctene.

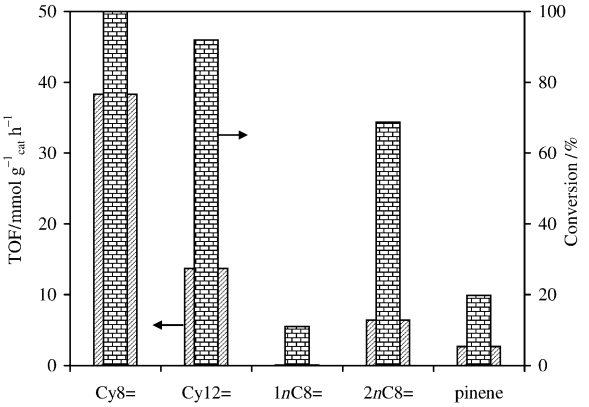

Figure 12. Oxidation of olefins using TBHP at 55 °C in the presence of MCM-41/**1**. The turnover frequency (TOF) was calculated at 1 h after the start of reaction and the substrate conversion at 24 h for cyclooctene (Cy8=); cyclododecene (Cy12=), 1-octene (1nC8=); *trans*-2-octene (2nC8=); α-pinene (Pinene).

The materials prepared in the presence of triethylamine, MCM-41/**1**/Et_3N and MCM-41/**2**/Et_3N gave worse results for the catalytic epoxidation of cyclooctene than those prepared in the absence of the amine. For MCM-41/**1**/Et_3N, the activity for the first run was higher than that for MCM-41/**2**/Et_3N, but for the second run there was a decrease in activity and both systems exhibited similar kinetic curves (Figure 11). The poor results were probably a consequence of the high metal loadings (approximately 4 wt.%). As discussed above, the EXAFS data point to the presence of oxo-bridged dinuclear species in as-made MCM-41/**1**/Et_3N. This may only represent the resting structure of the catalyst; that is, transformation to active monometallic species may take place in the presence of TBHP.[20] Leaching of active mononuclear species into solution would account for the drop in activity between the second and third runs. The system containing MCM-41/**1**/Et_3N is also unusual in that 1,2-cyclooctanediol is always formed as a secondary reaction product. Epoxide ring opening occurs when the Lewis acidity, provided by the Mo^{VI} metal centre and required for peroxide activation, suffices for converting the epoxide into the diol. If the interaction of Et_3N with the surface results in an increase in protonic acid strength of some silanol groups able to decompose the epoxide, then ring opening should also be observed in the presence of MCM-41/**2**/Et_3N, which is not the case. The production of 1,2-cyclooctanediol must instead be due to the formation of certain oxomolybdenum species during the reaction. A better understanding of this mechanism would require more detailed spectroscopic studies in situ, which are probably not worthwhile because of the relatively poor catalytic performance.

Catalytic oxidation of alcohols: The oxidation of alcohols to carbonyl compounds and carboxylic acids is a fundamental synthetic transformation. Molybdenum oxide-based catalysts have been used successfully as catalysts for the gas-phase oxidative dehydrogenation (ODH) of alcohols.[10d, 11a] Ruthenium complexes can oxidise alcohols effectively in the presence of basic TBHP; the reaction gives active intermediate *tert*-butylperoxoruthenium species, RuOO(*t*Bu), which are proton acceptors.[27] Species of this nature are also formed by the reaction of TBHP with molybdenum complexes $[MoO_2X_2L_2]$ (X = Cl, Br, CH_3), where L_2 is a Lewis base ligand.[18] Hence, we studied the catalytic potential of the derivatised MCM-41 materials in the liquid-phase oxidation of a range of primary and secondary benzylic and aliphatic alcohols, namely benzyl alcohol, *sec*-phenethyl alcohol, cyclohexanol, cyclooctanol, cyclohexylmethanol, 1-cyclohexylethanol, 1-octanol and (1*R*,2*S*,5*R*)-(−)-menthol. Control experiments were performed without a catalyst and, where necessary, the net conversion with catalyst was calculated by subtracting the non-catalytic contribution from the observed conversion (Table 4). Without TBHP no alcohol oxidation was observed. Pristine MCM-41 had no significant catalytic activity. All derivatised materials exhibited poor activity in the oxidation of primary aliphatic alcohols such as 1-octanol and cyclohexylmethanol, giving less than 3% conversion to the corresponding aldehyde. The most outstanding results were those obtained for the oxidation of secondary aliphatic and benzylic alcohols in the presence of MCM-41/**1**/Et_3N. Conversions at 24 h ranged from 43% to 59% and the corresponding carbonyl products were mainly formed (Table 4). A maximum TOF of 5.9 mmol $(g^{-1}cat)\,h^{-1}$ was observed for the oxidation of benzyl alcohol to benzaldehyde and benzoic acid (Figure 13). The latter was a secondary

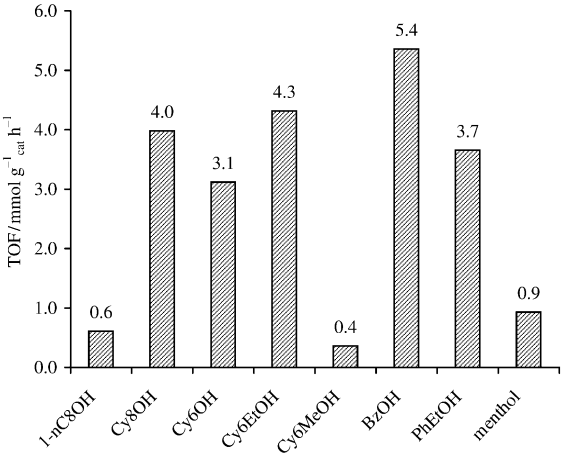

Figure 13. Oxidation of alcohols using TBHP at 55 °C in the presence of MCM-41/**1**/Et_3N. The TOF was calculated at 1 h after the start of reaction of 1-octanol (1-nC8OH), cyclooctanol (Cy8OH), cyclohexanol (Cy6OH), 1-cyclohexylethanol (Cy6EtOH), cyclohexylmethanol (Cy6MeOH), benzyl alcohol (BzOH), *sec*-phenethyl alcohol (PhEtOH) and (1*R*,2*S*,5*R*)-(−)-menthol (menthol).

Table 4. Alcohol oxidations using TBHP at 55 °C in the presence of MCM-41 materials.

Substrate	Catalyst	Conversion[a] [%]	Selectivity to carbonyl[b] [%]
Cy8OH	MCM-41/**1**	7	100
	MCM-41/**2**	7	100
	MCM-41/**1**/Et_3N (1st run)	53	100
	MCM-41/**1**/Et_3N (2nd run)	48	100
	MCM-41/**1**/Et_3N (3rd run)	38	100
	MCM-41/**2**/Et_3N	–	–
	no catalyst	29	100
Cy6OH	MCM-41/**1**	–	–
	MCM-41/**2**	2	100
	MCM-41/**1**/Et_3N	48	100
	MCM-41/**2**/Et_3N	–	–
	no catalyst	11	100
Cy6EtOH	MCM-41/**1**	6	100
	MCM-41/**2**	5	100
	MCM-41/**1**/Et_3N	43	100
	MCM-41/**2**/Et_3N	2	100
	no catalyst	12	100
PhEtOH	MCM-41/**1**	4	100
	MCM-41/**2**	6	100
	MCM-41/**1**/Et_3N	59	100
	MCM-41/**2**/Et_3N	8	100
	no catalyst	10	100
BzOH	MCM-41/**1**	2	89[c]
	MCM-41/**2**	12	85[c]
	MCM-41/**1**/Et_3N	45	67[c]
	MCM-41/**2**/Et_3N	19	100
	no catalyst	11	87[c]
menthol	MCM-41/**1**	10	100
	MCM-41/**2**	–	–
	MCM-41/**1**/Et_3N	10	100
	MCM-41/**2**/Et_3N	–	–
	no catalyst	2	100

[a] Substrate conversion after 24 h. In the presence of a catalyst the net conversion was corrected by subtracting the non-catalytic contribution from the observed conversion. [b] Calculated as: (number of moles of carbonyl product formed)/(total number of moles of products formed) × 100. [c] Benzoic acid was formed.

product resulting from the consecutive oxidation of benzaldehyde. This stepwise oxidation of benzyl alcohol was confirmed by carrying out the oxidation of benzaldehyde in the presence of MCM-41/**1**/Et_3N, which yielded 94% benzoic acid after 24 h.

The recyclability of MCM-41/**1**/Et_3N for cyclooctanol oxidation is comparable with that observed for cyclooctene epoxidation (Figure 14). Metal leaching was less than 5%. Water is a possible by-product formed in ODH, which may contribute to solvation of some metal species. Also shown in Figure 14 are the results obtained for cyclooctanol oxidation in the presence of the precursor complex $[MoO_2Cl_2(thf)_2]$, with a 1% molar ratio of catalyst/substrate. The kinetic curve is almost identical to that obtained without catalyst. This is another indication that the grafted metal species in MCM-41/**1**/Et_3N have a structure quite different from that of the precursor dioxomolybdenum(VI) complex.

For the reactions studied here, the formation of the aldehyde or ketone results from a nucleophilic attack on the alcohol group. Hence, the nucleophilic oxygen species should show high enough basicity to abstract hydrogen from the alcohol molecule. A distinctive feature of the MCM-41/**1**/Et_3N catalyst is the presence of oxo-bridged Mo dimers. Since the presence of other Mo species cannot be ruled out, it cannot be assumed that those species are totally responsible for the observed ODH activity. As mentioned above, dinuclear species may be partly transformed into monometallic species in the presence of TBHP. Marchi et al. studied the surface species of silica-supported molybdenum catalysts,[28] and reported that doping of the silica surface with sodium modified the surface properties, generating some species with molybdenum in tetrahedral coordination, which may be more reducible at lower temperatures than those formed on non-doped silica. Kikutani, in detailed EXAFS and UV/Vis spectroscopic studies on silica-supported molybdenum catalysts for the conversion of ethanol, showed that the reduction of the catalysts by the alcohol is a complicated process in which at least two distinctive states may be involved.[29] These findings indicate that a full understanding of the mechanisms of alcohol oxidation on supported catalysts is complicated and requires in-situ characterisation techniques and possibly labelled compounds.

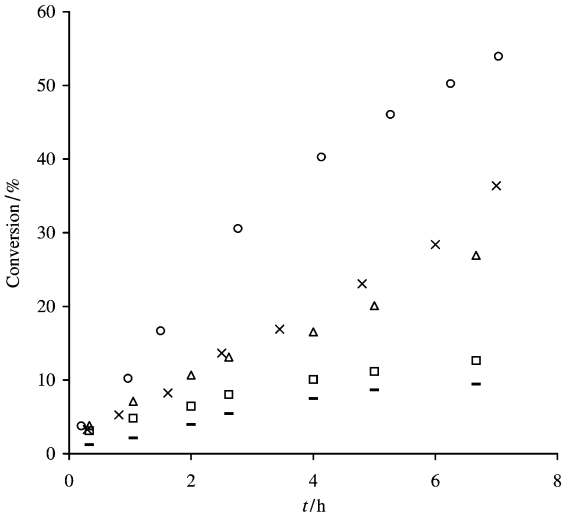

Figure 14. Conversion versus time curves for the oxidation of cyclooctanol using TBHP in the presence of MCM-41/**1**/Et_3N (○, 1st run; ×, 2nd run; △, 3rd run); $[MoO_2Cl_2(thf)_2]$ (□) and without a catalyst (–).

Concluding Remarks

Mesoporous silica MCM-41 derivatised with oxomolybdenum(VI) species can be prepared in a straightforward manner by grafting calcined MCM-41 with the complexes $[MoO_2X_2(thf)_2]$ (X = Cl, Br). EXAFS spectroscopy shows that these species are composed of isolated dioxomolybdenum(VI) groups at low loadings. The high dispersion of active sites appears to promote good catalytic activity for the epoxidation of olefins by TBHP. At higher loading, achieved using triethylamine to activate the surface silanol groups, the material formed with the dichloro complex contains dimeric or polymeric species. At the same high loading, the material formed with the dibromo complex contains more mononuclear than dinuclear sites, revealing that the complex has a quite different reactivity and surface chemistry. The materials

with the high metal loadings were not very active as catalysts for olefin epoxidation, but good results were obtained for the oxidation of secondary aliphatic and benzylic alcohols using the material containing oxo-bridged dimers. The actual catalytic species is likely to be formed by cleavage of the Mo–O–Mo bond by TBHP.

Experimental Section

Catalyst preparation: All preparations and manipulations were carried out using standard Schlenk techniques under nitrogen. Solvents were dried by standard procedures (THF, hexane and diethyl ether with Na/benzophenone; CH_2Cl_2 with CaH_2), distilled under nitrogen and kept over 4 Å molecular sieves. MoO_2Cl_2 and MoO_2Br_2 were obtained from Aldrich and used as received. The solvent adducts **1** and **2** were prepared as described previously.[30] Purely siliceous MCM-41 was synthesised using $[(C_{14}H_{29})N(CH_3)_3]Br$ as the templating agent.[31] Before the grafting experiments, physisorbed water was removed from calcined MCM-41 by heating it at 180 °C in vacuo (10^{-2} Pa) for 2 h.

In a typical grafting experiment, a solution of $[MoO_2X_2(thf)_2]$ (1 mmol) in CH_2Cl_2 (10 mL) was added to a stirred suspension of dry MCM-41 (1.0 g) in CH_2Cl_2 (10 mL). For MCM-41/**1** and MCM-41/**2**, the reaction mixture was stirred at ambient temperature overnight. For MCM-41/**1**/Et_3N and MCM-41/**2**/Et_3N, freshly distilled triethylamine (0.3 mL, 1.8 mmol) was added dropwise 30 min after the addition of the $[MoO_2X_2(thf)_2]$ solution. The reaction mixture was then stirred at ambient temperature overnight. The derivatised silicas were isolated by filtration, washed repeatedly with CH_2Cl_2, and dried in vacuo at ambient temperature for several hours.

MCM-41/1: elemental analysis found (%) for: Mo 1.1; IR (KBr): $\tilde{\nu}$ = 2982(w), 2886(w), 1230(s), 1077(vs), 965(m), 917(sh), 889(sh), 800(m), 573(m), 459(s).

MCM-41/2: elemental analysis found (%) for: Mo 0.5; IR (KBr): $\tilde{\nu}$ = 2979(w), 2894(w), 1226(s), 1071(vs), 956(m), 918(sh), 891(sh), 802(m), 567(m), 453(s).

MCM-41/1/Et$_3$N: elemental analysis found (%) for: Mo 4.0; IR (KBr): $\tilde{\nu}$ = 2990(m), 2793(m), 2730(m), 2693(m), 2494(m), 1474(m), 1398(m), 1385(w), 1233(s), 1080(vs), 949(m), 918(sh), 885(sh), 804(m), 577(m), 459(s).

MCM-41/2/Et$_3$N: elemental analysis found (%) for: Mo 3.9; IR (KBr): $\tilde{\nu}$ = 2986(m), 2787(m), 2726(m), 2689(m), 2490(m), 1475(m), 1398(m), 1385(w), 1079(vs), 965(w), 945 (m), 919(sh), 803(s), 566(m), 449(s).

Physical measurements: The molybdenum content in the samples was determined by ICP-AES. Powder XRD data were collected on a Philips X'pert diffractometer using $Cu_{K\alpha}$ radiation filtered by Ni. Data were collected at room temperature between $2^\circ \le 2\theta \le 12^\circ$ with a step size of 0.02° and a count time of 5 s/step. IR spectra in transmission mode were measured with a Mattson Mod 7000 FTIR spectrometer using KBr pellets. ^{13}C and ^{29}Si NMR spectra were recorded at 100.62 and 79.49 MHz, respectively, on a (9.4 T) Bruker Avance 400 spectrometer. ^{29}Si MAS NMR spectra were recorded with 40° pulses, spinning rates of 5.0–5.5 kHz, and 60 s recycle delays. ^{29}Si CP-MAS NMR spectra were recorded with 5.5 μs ^1H 90° pulses, 8 ms contact time, a spinning rate of 4.5 kHz and 4 s recycle delays. ^{13}C CP-MAS NMR spectra were recorded with a 4.5 μs ^1H 90° pulse, 2 ms contact time, a spinning rate of 8 kHz and 4 s recycle delays. Chemical shifts are stated in parts per million from tetramethylsilane (TMS).

Nitrogen adsorption–desorption isotherms were measured at 77 K in a gravimetric adsorption apparatus equipped with a CI electronic MK2-M5 microbalance and an Edwards Barocel pressure sensor. The out-gassing temperature was raised slowly (1 K min^{-1}) to 723 K for the pristine MCM-41 samples and to 413 K for the derivatised materials (to minimise destruction of the functionalities), and maintained at that temperature overnight at a residual pressure of approximately 10^{-4} mbar. The specific surface areas (S_{BET}) were calculated by applying the BET equation. The specific total pore volume (micropore plus mesopore, V_P) was estimated from the N_2 uptake at $p/p_0 \approx 0.95$. The pore size distribution (PSD) curves (the differential volume adsorbed with respect to the differential pore size per unit mass, plotted against pore width) were computed from the desorption branch of the experimental isotherms by a method based on the area of the pore walls.[32, 33] Assuming open cylindrical pores with radius r_p and zero contact angle, and correcting for the thickness of the layer already adsorbed, r_p can be calculated by summing the Kelvin radius and the statistical average thickness (t, calculated using the Halsey equation) of the adsorbed layer.

Mo *K*-edge X-ray absorption spectra were measured at room temperature in transmission mode on beamline BM29 at the ESRF (Grenoble),[34] operating at 6 GeV in ⅔ filling mode with typical currents of 170–200 mA. One scan was performed for each sample and set up to record the pre-edge at 5 eV steps and the post-edge region in 0.025–0.05 Å^{-1} steps, giving a total acquisition time of approximately 45 min per scan. The order-sorting double Si(311) crystal monochromator was detuned by 40% to ensure harmonic rejection. Solid samples were diluted with BN and pressed into 13 mm pellets. Ionisation chamber detectors were filled with Kr to give 30% absorbing I_0 (incidence) and 70% absorbing I_t (transmission). The programs EXCALIB and EXBACK (SRS Daresbury Laboratory, UK) were used in the usual manner for calibration and background subtraction of the raw data. EXAFS curve-fitting analyses, by least-squares refinement of the non-Fourier filtered k^3-weighted EXAFS data, were carried out using the program EXCURVE (version EXCURV98[35]), applying fast curved wave theory.[36] Phase shifts were obtained within this program using ab-initio calculations based on the Hedin–Lundqvist/von Barth scheme. The calculations were performed with single scattering only.

Catalytic oxidation reactions: The liquid-phase oxidation of cyclooctene was carried out at 55 °C under an air atmosphere, in a micro reaction vessel equipped with a magnetic stirrer. The reactor was loaded with catalyst (175 mg), cyclooctene (7.3 mmol) and *tert*-butyl hydroperoxide (11 mmol) as oxidant (5.5 M in decane). Samples were withdrawn periodically and analysed using a gas chromatograph (Varian 3800) equipped with a capillary column (DB-5, 30 m × 0.25 mm for olefin epoxidation and CP WAX 52CB, 30 m × 0.53 mm for alcohol oxidation) and a flame ionisation detector. The products were quantified using calibration curves and *n*-nonane or undecane as internal standard (added after the reaction). Catalysts were recycled by recovering the solids by filtration, washing them thoroughly with dichloromethane and drying them at room temperature overnight.

Acknowledgements

This work was partly funded by the FCT, POCTI and FEDER (Project PCTI/1999/QUI/32889). A.A.V. and M.P. thank the FCT for post-doctoral grants, and C.N. thanks the University of Aveiro and the FCT for doctoral grants. We acknowledge the European Synchrotron Radiation Facility for provision of synchrotron radiation facilities and we thank Stuart Ansell for assistance in using beamline BM29.

[1] a) M. A. Banares, I. E. Wachs, *J. Raman Spectrosc.* **2002**, *33*, 359; b) M. A. Banares, *Catal. Today* **1999**, *51*, 319; c) N. C. Ramani, D. L. Sullivan, J. G. Ekerdt, J. M. Jehng, I. E. Wachs, *J. Catal.* **1998**, *176*, 143; d) M. A. Banares, L. J. Alemany, M. L. Granados, M. Faraldos, J. L. G. Fierro, *Catal. Today* **1997**, *33*, 73; e) I. E. Wachs, *Catal. Today* **1996**, *27*, 437;f) I. E. Wachs, G. Deo, M. A. Vuurman, H. C. Hu, D. S. Kim, J. M. Jehng, *J. Mol. Catal.* **1993**, *82*, 443.

[2] Y. Iwasawa, in *Tailored Metal Catalysts* (Ed.: Y. Iwasawa), D. Riedel, Dordrecht, **1986**, pp. 1–85.

[3] a) J. Y. Ying, C. P. Mehnert, M. S. Wong, *Angew. Chem.* **1999**, *111*, 58; *Angew. Chem. Int. Ed.* **1999**, *38*, 56; b) U. Ciesla, F. Schüth, *Micropor. Mesopor. Mater.* **1999**, *27*, 131; c) X. He, D. Antonelli, *Angew. Chem.* **2002**, *114*, 222; *Angew. Chem. Int. Ed.* **2002**, *41*, 214.

[4] a) A. Corma, *Chem. Rev.* **1997**, *97*, 2373; b) A. Sayari, *Chem. Mater.* **1996**, *8*, 1840.

[5] a) C. T. Kresge, M. E. Leonowicz, W. J. Roth, J. C. Vartuli, J. S. Beck, *Nature* **1992**, *359*, 710; b) J. S. Beck, J. C. Vartuli, W. J. Roth, M. E. Leonowicz, C. T. Kresge, K. D. Schmitt, C. T.-W. Chu, D. H. Olson, E. W. Sheppard, S. B. McCullen, J. B. Higgins, J. L. Schlenker, *J. Am. Chem. Soc.* **1992**, *114*, 10834.

[6] Q. Huo, D. I. Margolese, G. D. Stucky, *Chem. Mater.* **1996**, *8*, 1147.

[7] S. Inagaki, Y. Fukushima, K. Kuroda, *J. Chem. Soc. Chem. Commun.* **1993**, 680.
[8] a) K. Moller, T. Bein, *Chem. Mater.* **1998**, *10*, 2950; b) T. Maschmeyer, *Curr. Opin. Solid State Mater. Sci.* **1998**, *3*, 71; c) D. E. De Vos, M. Dams, B. F. Sels, P. A. Jacobs, *Chem. Rev.* **2002**, *102*, 3615.
[9] a) M. S. Morey, J. D. Bryan, S. Schwarz, G. D. Stucky, *Chem. Mater.* **2000**, *12*, 3435; b) M. S. Morey, A. Davidson, H. Eckert, G. D. Stucky, *Chem. Mater.* **1996**, *8*, 486; c) P. VanDerVoort, M. S. Morey, G. D. Stucky, M. Mathieu, E. F. Vansant, *J. Phys. Chem. B* **1998**, *102*, 585; d) M. S. Morey, S. Schwarz, M. Fröba, G. D. Stucky, *J. Phys. Chem. B* **1999**, *103*, 2037; e) M. S. Morey, A. Davidson, G. D. Stucky, *Micropor. Mater.* **1996**, *6*, 99; f) M. S. Morey, S. O'Brien, S. Schwarz, G. D. Stucky, *Chem. Mater.* **2000**, *12*, 898.
[10] a) T. Maschmeyer, F. Rey, G. Sankar, J. M. Thomas, *Nature* **1995**, *378*, 159; b) L. Marchese, E. Gianotti, V. Dellarocca, T. Maschmeyer, F. Rey, S. Coluccia, J. M. Thomas, *Phys. Chem. Chem. Phys.* **1999**, *1*, 585; c) P. Ferreira, I. S. Gonçalves, F. E. Kühn, M. Pillinger, J. Rocha, A. M. Santos, A. Thursfield, *Eur. J. Inorg. Chem.* **2000**, 551; d) I. J. Shannon, T. Maschmeyer, R. D. Oldroyd, G. Sankar, J. M. Thomas, H. Pernot, J.-P. Balikdjian, M. Che, *J. Chem. Soc. Faraday Trans.* **1998**, *94*, 1495.
[11] a) M. Seman, J. N. Kondo, K. Domen, R. Radhakrishnan, S. T. Oyama, *J. Phys. Chem. B* **2002**, *106*, 12965; b) S. Takenaka, T. Tanaka, T. Funabiki, S. Yoshida, *J. Phys. Chem. B* **1998**, *102*, 2960; c) G. Mestl, T. K. K. Srinivasan, *Catal. Rev.—Sci. Eng.* **1998**, *40*, 451; d) F. Arena, A. Parmaliana, *J. Phys. Chem.* **1996**, *100*, 19994; e) M. Faraldos, M. A. Banares, J. A. Anderson, H. C. Hu, I. E. Wachs, J. L. G. Fierro, *J. Catal.* **1996**, *160*, 214; f) H. C. Hu, I. E. Wachs, *J. Phys. Chem.* **1995**, *99*, 10911; g) M. A. Banares, H. C. Hu, I. E. Wachs, *J. Catal.* **1994**, *150*, 407; h) A. Parmaliana, V. Sokolovskii, D. Miceli, F. Arena, N. Giordano, *J. Catal.* **1994**, *148*, 514.
[12] P. Ferreira, I. S. Gonçalves, F. E. Kühn, A. D. Lopes, M. A. Martins, M. Pillinger, A. Pina, J. Rocha, C. C. Romão, A. M. Santos, T. M. Santos, A. A. Valente, *Eur. J. Inorg. Chem.* **2000**, 2263.
[13] a) X. S. Zhao, G. Q. Lu, A. K. Whittaker, G. J. Miller, H. Y. Zhu, *J. Phys. Chem. B* **1997**, *101*, 6525; b) P. L. Llewellyn, F. Schüth, Y. Grillet, F. Rouquerol, J. Rouquerol, K. K. Unger, *Langmuir* **1995**, *11*, 574.
[14] a) B. Marler, U. Oberhagemann, S. Voltmann, H. Gies, *Micropor. Mater.* **1996**, *6*, 375; b) W. Hammond, E. Prouzet, S. D. Mahanti, T. J. Pinnavaia, *Micropor. Mesopor. Mater.* **1999**, *27*, 19.
[15] G. Sankar, M. A. Roberts, J. M. Thomas, G. U. Kulkarni, N. Rangavittal, C. N. R. Rao, *J. Solid State Chem.* **1995**, *119*, 210.
[16] S. P. Cramer, K. O. Hodgson, W. O. Gillum, L. E. Mortenson, *J. Am. Chem. Soc.* **1978**, *100*, 3398.
[17] J. Evans, J. T. Gauntlett, J. F. W. Mosselmans, *Faraday Discuss. Chem. Soc.* **1990**, 107.
[18] F. E. Kühn, M. Groarke, É. Bencze, E. Herdtweck, A. Prazeres, A. M. Santos, M. J. Calhorda, C. C. Romão, I. S. Gonçalves, A. D. Lopes, M. Pillinger, *Chem. Eur. J.* **2002**, *8*, 2370.
[19] M. Cindrić, N. Strukan, V. Vrdoljak, M. Devčić, Z. Veksli, B. Kamenar, *Inorg. Chim. Acta* **2000**, *304*, 260.
[20] S. Leinonen, D. C. Sherrington, A. Sneddon, D. McLoughlin, J. Corker, C. Canevali, F. Morazzoni, J. Reedijk, S. B. D. Spratt, *J. Catal.* **1999**, *183*, 251.
[21] G. N. Schrauzer, L. A. Hughes, N. Strampach, *Z. Naturforsch. B* **1982**, *37*, 380.
[22] M. S. Rau, C. M. Kretz, G. L. Geoffroy, A. L. Rheingold, *Organometallics* **1993**, *12*, 3447.
[23] a) D. Saurenz, F. Demirhan, P. Richard, R. Poli, H. Sitzmann, *Eur. J. Inorg. Chem.* **2002**, 1415; b) E. Collange, J. A. Garcia, R. Poli, *New J. Chem.* **2002**, *26*, 1249.
[24] H. Arzoumanian, R. Lai, S. Le Bot, M. Pierrot, F. Ridouane, *Inorg. Chim. Acta* **1991**, *182*, 173.
[25] F. E. Kühn, E. Herdtweck, J. J. Haider, W. A. Herrmann, I. S. Gonçalves, A. D. Lopes, C. C. Romão, *J. Organomet. Chem.* **1999**, *583*, 3.
[26] a) F. E. Kuhn, A. D. Lopes, A. M. Santos, E. Herdtweck, J. J. Haider, C. C. Romão, A. G. Santos, *J. Mol. Catal. A: Chem.* **2000**, *151*, 147; b) F. E. Kuhn, A. M. Santos, A. D. Lopes, I. S. Gonçalves, E. Herdtweck, C. C. Romão, *J. Mol. Catal. A: Chem.* **2000**, *164*, 25.
[27] W.-H. Fung, W.-Y. Yu, C.-M. Che, *J. Org. Chem.* **1998**, *63*, 2873.
[28] A. J. Marchi, E. J. Lede, F. G. Requejo, M. Rentería, S. Irusta, E. A. Lombardo, E. E. Miro, *Catal. Lett.* 1997, **48**, 47.
[29] Y. Kikutani, *J. Mol. Catal. A: Chem.* **1999**, *142*, 247.
[30] W. M. Carmichael, D. A. Edwards, G. W. A. Fowles, P. R. Marshall, *Inorg. Chim. Acta* **1967**, *1*, 93.
[31] C. D. Nunes, A. A. Valente, M. Pillinger, A. C. Fernandes, C. C. Romão, J. Rocha, I. S. Gonçalves, *J. Mater. Chem.* **2002**, *12*, 1735.
[32] S. J. Gregg, K. S. W. Sing, *Adsorption, Surface Area and Porosity*, 2nd ed., Academic Press, London, **1982**.
[33] J. M. Thomas, W. J. Thomas, *Principles and Practice of Heterogeneous Catalysis*, Wiley–VCH, Weinheim, **1997**.
[34] A. Filipponi, M. Borowski, D. T. Bowron, S. Ansell, A. D. Cicco, S. D. Panfilis, J.-P. Itiè, *Rev. Sci. Instrum.* **2000**, *71*, 2422.
[35] N. Binsted, EXCURV98, CCLRC Daresbury Laboratory, Warrington (UK), **1998**.
[36] a) S. J. Gurman, N. Binsted, I. Ross, *J. Phys. C* **1984**, *17*, 143; b) S. J. Gurman, N. Binsted, I. Ross, *J. Phys. C* **1986**, *19*, 1845.

Received: February 20, 2003 [F4887]